NÖHÜ Müh. Bilim. Derg. / NOHU J. Eng. Sci., 17 (2026), 1909194
Niğde Ömer Halisdemir Üniversitesi Mühendislik Bilimleri Dergisi
Niğde Ömer Halisdemir University Journal of Engineering Sciences
Araştırma makalesi / Research article
www.dergipark.org.tr/tr/pub/ngumuh / www.dergipark.org.tr/en/pub/ngumuh

Strain rate–dependent tensile behavior of high-density polyethylene: Experimental characterization and finite element modeling

Yüksek yoğunluklu polietilenin gerinme hızına bağlı çekme davranışı: Deneysel karakterizasyon ve sonlu elemanlar modellemesi

Vahit Keyfli[1], Zakir Taş[2], Mehmet Akif Dündar[3], Kazım Ercan[4*], Osman Özenç[5]

[1,2,3,4,5] *Department of Mechanical Engineering, College of Engineering, Yozgat Bozok University, Yozgat, Türkiye*

Abstract

This study investigated the tensile behavior of high-density polyethylene (HDPE) at different strain rates using experiments and finite element analysis. Uniaxial tensile tests were conducted at strain rates from 5 × 10-3 to 5 × 10-1 s-1, revealing clear rate sensitivity. The elastic modulus and true tensile yield stress increased with strain rate, while fracture strain decreased, indicating reduced ductility at higher rates. Finite element simulations in ABAQUS applied a linear Drucker–Prager model with a Von Mises yield surface combined with the Cowper–Symonds equation. The model captured the rate-dependent increase in yield stress and the overall post-yield response. However, strain hardening at higher strain rates was overestimated because the hardening curve was defined at the lowest strain rate and the modulus was assumed rate-independent. Overall, the framework provides an efficient approach for predicting the tensile response of HDPE, though incorporating rate-dependent hardening and viscoelasticity would improve post-yield predictions.

Keywords: High-density polyethylene (HDPE), Tensile behavior, Strain rate, Drucker-Prager, Finite element analysis

Öz

Bu çalışmada, deneyler ve sonlu elemanlar analizi kullanılarak farklı gerinim hızlarında yüksek yoğunluklu polietilenin (HDPE) gerilme davranışı incelenmiştir. 5 × 10-3 ila 5 × 10-1 s-1 gerinim hızlarında tek eksenli gerilme testleri gerçekleştirilmiş ve net bir hız duyarlılığı ortaya çıkmıştır. Elastik modül ve gerçek çekme akma gerilimi gerinim hızı ile artarken, kırılma gerinimi azalmış ve bu da daha yüksek hızlarda sünekliğin azaldığını göstermiştir. ABAQUS'ta yapılan sonlu eleman simülasyonlarında, Cowper-Symonds denklemi ile birleştirilmiş Von Mises akma yüzeyi ile doğrusal Drucker-Prager modeli uygulanmıştır. Model, akma geriliminin hız bağımlı artışını ve genel akma sonrası tepkiyi yakaladı. Ancak, sertleşme eğrisi en düşük gerilme hızında tanımlandığından ve modülün hızdan bağımsız olduğu varsayıldığından, daha yüksek gerilme hızlarında gerilme sertleşmesi fazla tahmin edildi. Genel olarak, çerçeve HDPE'nin çekme tepkisini tahmin etmek için verimli bir yaklaşım sağlar, ancak hız bağımlı sertleşme ve viskoelastisiteyi dahil etmek akma sonrası tahminleri iyileştirecektir.

Anahtar kelimeler: Yüksek yoğunluklu polietilen (HDPE), Çekme davranışı, Gerilme hızı, Drucker-Prager, Sonlu elemanlar analizi

1 Introduction

The use of polymeric materials and their composites have increased significantly across multiple industries, particularly in the automotive sector, primarily due to their lightweight nature and superior corrosion resistance compared to metals [1–4]. Among thermoplastics, polyethylene (PE) is the most widely produced polymer worldwide, owing to its favorable combination of toughness, abrasion and impact resistance, near-zero waters absorption, low cost, and recyclability [2, 5]. These attributes make polyethylene a highly attractive material for large-scale structural and non-structural applications [6]. Polyethylene is classified into low-density (LDPE), medium-density (MDPE), and high-density polyethylene (HDPE) based on variations in molecular structure and degree of crystallinity [2]. Among these types, HDPE exhibits comparatively greater stiffness, strength, and enhanced resistance to creep deformation, enabling improved load-carrying capacity and long-term structural stability. Reflecting these advantageous properties, worldwide consumption of HDPE has increased markedly, rising from 11.9 million tons in 1990 to 43.9 million tons in 2017, with an average annual growth rate of approximately 3.3% [2]. Owing to its favorable mechanical performance and chemical durability, HDPE is widely employed in packaging applications, storage and pressure vessels, piping systems, automotive parts, and numerous industrial products [7, 8]. The synergy of strength, environmental resistance, economic efficiency, and recyclability establishes HDPE as a key engineering thermoplastic for large-scale production and infrastructure-related uses [6]. However, these advantageous attributes alone do not guarantee reliable structural performance. In practical service conditions—ranging from quasi-static loading in buried pipelines to impact-dominated events in protective components [9]. HDPE is frequently subjected to varying strain rates that can substantially alter its mechanical

* Sorumlu yazar / Corresponding author, e-posta / e-mail: kazim.ercan@yobu.edu.tr (K. Ercan)
Geliş / Received: 13.03.2026 Kabul / Accepted: 02.05.2026 Yayımlanma / Published: 16.06.2026
doi: 10.28948/ngumuh.1909194

response. Furthermore, HDPE, like many engineering materials, exhibits a highly non-linear stress–strain response [3], strongly influenced by molecular mobility and time-dependent viscoelastic–viscoplastic mechanisms [6, 10]. As a semi-crystalline polymer, its tensile behavior arises from the interplay between crystalline lamellae and amorphous regions [11]. Initial elastic stretching is followed by yield due to lamellar slip, interlamellar shear, and localized plastic flow within the amorphous phase [12, 13], often leading to neck formation rather than uniform strain softening [12, 14]. Continued deformation aligns molecular chains and crystalline structures, producing pronounced strain hardening [14, 15]. These microstructurally driven, rate-sensitive mechanisms make simple linear or rate-independent models inadequate, highlighting the need to rigorously characterize HDPE's strain rate–dependent tensile behavior for reliable design and material modeling.

The tensile response of HDPE is consistently reported to be strongly strain rate dependent, even within the quasi-static regime. In the range of 7.25×10^{-5} – 7.25×10^{-3} s^{-1}, Reis et al. [16] observed clear rate-induced increases in elastic modulus and tensile yield strength, accompanied by reduced ductility, highlighting positive rate sensitivity. Similarly, Lamri et al. [17] reported that increasing strain rate led to a noticeable rise in yield stress and stiffness, which was attributed to limited molecular relaxation and suppressed viscoelastic deformation at higher loading rates. In addition, Amjadi and Fatemi [18] reported progressive stiffening and strengthening of HDPE with increasing strain rate, further confirming its pronounced rate-sensitive tensile behavior. Collectively, these studies emphasize that the tensile performance of HDPE is intrinsically governed by loading rate, necessitating rate-dependent constitutive formulations for reliable prediction [16–18]. Consistent with these observations, Dasari and Misra [19] demonstrated that HDPE exhibits a high strain rate sensitivity index, indicating a strong dependence of flow stress on applied strain rate even within moderate quasi-static loading conditions. Their results showed systematic increases in yield stress and post-yield flow stress with increasing strain rate, while the characteristic deformation sequence—elastic response, yielding, cold drawing, and strain hardening—remained preserved. Microstructural analysis revealed that higher strain rates promote enhanced fibrillar orientation and alignment within the drawn regions, contributing to increased resistance to plastic flow [19]. Furthermore, Reis et al. [20] showed in post-consumer recycled HDPE that increasing strain rate systematically increased the maximum true stress and initial stiffness while reducing ductility, indicating a transition toward a more brittle-like tensile response at higher loading rates due to constrained molecular relaxation processes. Dusunceli and Colak [21] performed systematic uniaxial tensile experiments on HDPE at room temperature over strain rates of 1×10^{-5}, 1×10^{-4}, and 1×10^{-3} s^{-1}, revealing a distinctly rate-sensitive mechanical response. Their findings demonstrated that strain rate exerts a significant influence across both the elastic and post-yield regimes, with increasing strain rate leading to elevated yield stress and higher flow stress at equivalent strain levels. Notably, the rate dependence was not confined to initial yielding but persisted throughout plastic deformation, underscoring the time-dependent nature of the underlying molecular mechanisms. Furthermore, their analysis indicated that conventional elastic–plastic constitutive descriptions are inadequate for accurately representing the observed behavior, thereby highlighting the necessity of incorporating viscoplastic formulations capable of capturing overstress and rate-controlled deformation effects. Dusunceli and Colak [22] further investigated the effect of manufacturing techniques on the time-dependent tensile behavior of HDPE using extruded pipe and compression-molded sheet specimens from the same raw material. Tensile loading–unloading tests conducted at strain rates of 1×10^{-5}, 1×10^{-4}, and 1×10^{-3} s^{-1} revealed clear viscoelastic and viscoplastic rate sensitivity, with higher strain rates producing increased stress and stiffness. Notably, extruded specimens exhibited more pronounced nonlinear behavior than compression-molded samples, reflecting differences in crystallinity and molecular orientation induced by processing.

Although the above studies have provided valuable insights into the strain rate-dependent tensile behavior of HDPE, they are largely limited to very low quasi-static strain rates or specific material grades, and they often focus on developing new constitutive models rather than systematically evaluating the predictive capability of widely used commercial models. Consequently, there remains a significant gap in experimental data covering intermediate-to-moderate strain rates up to 5×10^{-1} s^{-1}, as well as in the quantification of the strain rate sensitivity parameter across this broader range.

The present study addresses these gaps by experimentally investigating HDPE at strain rates of 5×10^{-3}, 1×10^{-2}, 1×10^{-1}, and 5×10^{-1} s^{-1}, and by determining the strain rate sensitivity using the Cowper-Symonds model. Additionally, the Drucker-Prager material model in Abaqus is employed to reproduce the full nonlinear stress–strain response, while effectively capturing a Von Mises yield surface. By integrating rigorous experimental characterization with computational validation, this work not only extends the findings of the above studies to higher and intermediate strain rates but also provides a practical and reliable framework for finite element analysis of HDPE under rate-dependent loading, offering both mechanistic understanding and engineering utility.

2 Materials and method

2.1 Material

The experimental specimens in this study were prepared from PE300-type HDPE with material code 100143009, in accordance with the DIN EN ISO 14632 TG3 standard. PE300 is a semi-crystalline thermoplastic with a homogeneous structure, distinguished by its high mechanical strength, dimensional stability, impact resistance, chemical durability, and excellent processability, making it widely used in industrial applications. The material was supplied by a local vendor in white plates measuring $2 \times 1 \times 0.004$ m and processed via extrusion. Its reported density is 0.95 g/cm³.

2.2 *Uniaxial tension tests*

Tensile test specimens were prepared from the HDPE plates in accordance with ASTM D638-14 Type V [23] using waterjet cutting. The actual specimen is shown in Figure 1(a), while Figure 1(b) provides the detailed geometric specifications. Although previous studies on blow-molded HDPE have reported a small anisotropy in elastic modulus—approximately 8% higher along the extrusion direction compared to the perpendicular direction [24] such orientation effects are generally less pronounced in extruded HDPE. Therefore, in this study, specimens were cut without consideration of orientation relative to the extrusion direction.

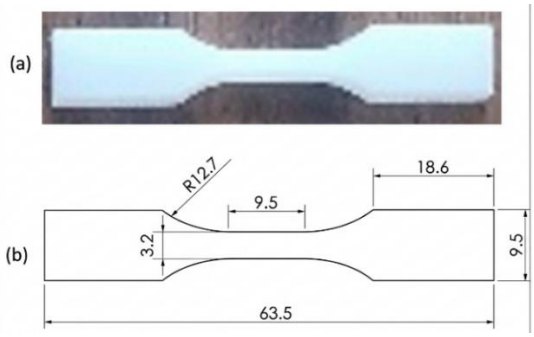

Figure 1. (a) Actual dog-bone shaped HDPE tensile test specimen with 4 mm thickness, prepared according to ASTM D638-14 Type V [23]; (b) Geometric specifications of the test specimen.

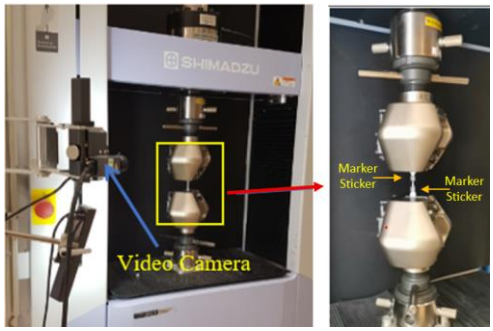

Figure 2. Experimental setup for uniaxial tension tests.

Uniaxial tensile tests on the HDPE specimens were conducted at four distinct elongation speeds of 5 x 10-2, 1 x 10-1, 1 x 100, and 5 x 100 mm/s, corresponding to nominal strain rates of 5 x 10-3, 1 x 10-2, 1 x 10-1, and 5 x 10-1 s^{-1}, respectively. Tests were performed using a SHIMADZU AGS-X universal testing machine, and strain measurements were obtained with a TRViewX advanced non-contact video extensometer, which enabled precise tracking of specimen deformation. Marker stickers depicted in Figure 2 were applied to the specimens to monitor displacement changes and calculate engineering strain accurately. The experimental setup is illustrated in Figure 2. All tests were conducted at room temperature (23°C), with at least five repetitions for each strain rate to ensure statistical reliability. Engineering stress–strain curves were generated using Shimadzu Trapezium-X software.

The engineering stress, σ_eng, was calculated using the standard formula, as given below.

$$\sigma_{eng} = F/A_0 \tag{1}$$

where F represents the applied load, and A_0 denotes the initial, undeformed cross-sectional area of the HDPE specimen. However, this engineering stress formulation does not account for changes in cross-sectional area or volume during deformation [25–27] and therefore may not accurately represent yielding and plastic flow behavior in polymers [28, 29]. Thus, to obtain a more precise description of the material response, particularly in the post-yield regime, the true stress–true strain relationship was calculated. True stress–true strain data provide a more accurate representation of the HDPE deformation behavior, capturing nonlinearities associated with necking and strain hardening. The true stress and true strain were computed using the standard relations for polymers as detailed in the following expressions [30, 31].

$$\sigma_{\mathrm{True}} = \sigma_{\mathrm{eng}}\left(1 + \varepsilon_{\mathrm{eng}}\right) \tag{2}$$

$$\varepsilon_{\mathrm{True}} = \ln\left(1 + \varepsilon_{\mathrm{eng}}\right) \tag{3}$$

where σ_{True} and $\varepsilon_{\mathrm{True}}$ represent the true stress (Cauchy stress) and true strain (logarithmic strain), respectively, while $\varepsilon_{\mathrm{eng}}$ represents the engineering strain. From the true stress–true strain data, the key mechanical properties of HDPE—including the true tensile elastic modulus and true tensile yield strength, and the corresponding strains were determined for each tested strain rate. The yield strength was identified by locating the local maximum stress and corresponding strain from the engineering stress–strain curves and converting these values to true stress and true strain using Equation (2) and Equation (3), respectively. These calculations assume material incompressibility and uniform deformation, without localized necking. To provide a more precise assessment of the onset of plastic deformation, the offset yield point was determined using a strain offset of 0.2% [29]. The strain rate corresponding to each elongation speed was calculated from the strain–time data recorded by the TRViewX non-contact video extensometer using the following relation [32].

$$\dot{\varepsilon} = \frac{d\varepsilon}{dt} = \frac{1}{L_0} \cdot \frac{dL}{dt} \tag{4}$$

Herein, $\dot{\varepsilon}$ is the strain rate, and L_0 and L are the initial and instantaneous lengths of the gauge section, respectively. This approach ensures accurate determination of the nominal strain rate for each test and allows the evaluation of rate-dependent mechanical properties across all tested conditions.

3 Finite element analysis

Finite element simulations were performed to reproduce the strain rate-dependent uniaxial tensile response of HDPE specimens and to support interpretation of the experimental

results. The analyses were conducted using Abaqus Standard/3D [33], employing implicit static procedures suitable for quasi-static and rate-dependent nonlinear problems [34, 35]. Both geometric and material nonlinearities were considered in all simulations. Geometric nonlinearity was incorporated to account for large deformations and cross-sectional area reduction occurring during tensile loading. Material nonlinearity was introduced through an elasto-plastic constitutive framework capable of capturing the yielding and post-yield hardening behavior of HDPE [35].

The material response was modeled using the Drucker–Prager plasticity model. For the present study, the parameters were selected such that the Drucker–Prager formulation reproduces a von Mises–type yield surface under uniaxial tension [35, 36]. This approach is appropriate since the experimental program focused exclusively on uniaxial tensile loading, where pressure sensitivity effects are not dominant. Consequently, the adopted formulation ensures consistency with the observed tensile behavior while maintaining numerical robustness.

Isotropic hardening was defined using the true stress–true strain curve obtained from the tensile test conducted at the lowest strain rate (5×10^{-3} s^{-1}). This curve was assumed to represent the quasi-static reference response of the material and was directly implemented to describe post-yield plastic hardening.

Strain-rate dependency was incorporated through the Cowper–Symonds overstress model [35, 37]. The dynamic yield stress was scaled as a function of plastic strain rate using calibrated Cowper–Symonds parameters, enabling the simulations to capture the experimentally observed rate sensitivity of HDPE. This formulation allows the quasi-static hardening curve to be extended to higher strain rates while preserving the underlying plastic flow characteristics.

Overall, the adopted modeling framework provides a consistent representation of the nonlinear tensile behavior of HDPE, accounting for large deformations, plastic hardening, and strain-rate effects within a unified finite element formulation.

3.1 Mesh, Element type, loading and boundary conditions

The finite element model of the uniaxial tensile specimen is illustrated in Figure 3, where (a) presents the three-dimensional discretized geometry and (b) shows the corresponding two-dimensional representation. The specimen geometry was modeled in accordance with the experimental configuration, with particular attention given to the gage section, where uniform stress and strain development is expected.

A structured hexahedral mesh was generated using eight-node linear brick elements with reduced integration and hourglass control (C3D8R) [38]. This element type is well suited for nonlinear implicit analyses involving large deformations and elastoplastic material behavior, offering a favorable compromise between computational efficiency and numerical accuracy. Reduced integration mitigates volumetric locking, which is particularly relevant for polymeric materials undergoing plastic flow, while hourglass control ensures stable element performance.

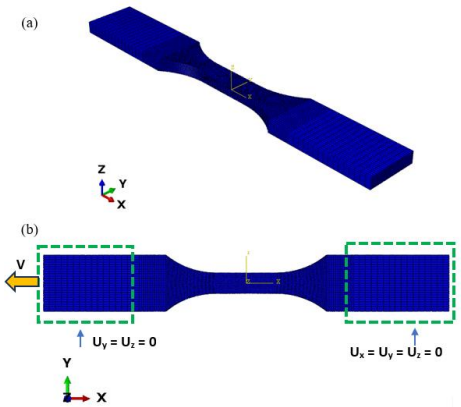

Figure 3. Finite element model of the uniaxial tension tests, (a) 3-D representation, and (b) 2-D representation

The final discretization comprised 39400 nodes and 32928 elements. Mesh refinement was concentrated along the gage length to accurately capture strain gradients and potential localization phenomena. The average element aspect ratio in this critical region was maintained at 1.14, indicating near-cubic elements and minimizing mesh-induced bias in the predicted stress–strain response. The adopted mesh density was verified to provide stable and mesh-independent global force–displacement results.

Boundary conditions were defined to replicate the experimental gripping configuration and to enforce a state of uniaxial deformation. One end of the specimen was fully constrained in all translational degrees of freedom, representing the fixed grip. The opposite end (Figure 3b) was constrained in the transverse directions and permitted to translate only along the loading axis. This constraint configuration suppresses rigid body motion while preventing unintended lateral displacement, ensuring that axial loading is the sole driving deformation mode.

Loading was applied in a displacement-controlled manner to reflect the experimental crosshead motion. Three elongation rates—0.05 mm/s, 1 mm/s, and 5 mm/s were imposed at the loading end. The use of displacement control enhances numerical stability in simulations involving post-yield softening or nonlinear plastic evolution. The prescribed velocities were selected to correspond directly to the experimental strain-rate conditions, thereby enabling consistent validation of the rate-dependent constitutive model within the implicit solution framework.

3.2 Material model

The linear Drucker–Prager constitutive model was adopted to represent the elastoplastic response of HDPE under uniaxial tensile loading. Although originally formulated to capture pressure-dependent yielding, the model can be parameterized to reproduce a von Mises–type response in cases where hydrostatic sensitivity is not dominant, such as uniaxial tension [39]. This makes it suitable for describing the nonlinear tensile behavior of polymeric materials within the present study. The

formulation enables representation of elastic–plastic transition and subsequent hardening behavior observed in the tensile stress–strain response. For the uniaxial tension case considered here, model parameters were calibrated to ensure consistency with the experimentally measured yield and post-yield response [35].

For an isotropic material, the linear Drucker–Prager yield function, F, can be defined in the following form [36].

$$F = \sigma_e + \alpha\sigma_m - \sigma_0 \tag{5}$$

In this formulation, σ_0 denotes the hardening parameter, which is directly related to the shear yield stress, σ_s, through the following relationship [34].

$$\sigma_o = \sqrt{3}\sigma_s \tag{6}$$

Here, σ_e and σ_m represent the effective (deviatoric) shear stress and the hydrostatic (mean) stress, respectively, and are defined in terms of the principal stresses, σ_1, σ_2, and σ_3, as given below [36].

$$\sigma_e = \left\{\frac{1}{2}[(\sigma_1 - \sigma_2)^2 + (\sigma_2 - \sigma_3)^2 + (\sigma_3 - \sigma_1)^2]\right\}^{1/2} \tag{7}$$

$$\sigma_m = \frac{1}{3}(\sigma_1 + \sigma_2 + \sigma_3) \tag{8}$$

In Equation (5), α represents the hydrostatic pressure sensitivity parameter and is calculated using the following expression [40].

$$\alpha = 3\left(\frac{\sigma_c - \sigma_t}{\sigma_c + \sigma_t}\right) \tag{9}$$

Here, σ_t and σ_c denote the tensile and compressive yield stresses corresponding to the same level of plastic strain, respectively. It is important to note that when $\sigma_t = \sigma_c$, the numerator becomes zero, resulting in $\alpha=0$. This corresponds to a pressure-insensitive (von Mises) yield behavior, which is consistent with the assumption for uniaxial tensile loading in the present study.

Equation (5), can also be rewritten in the equivalent form shown below [36]:

$$F = \sigma_e + \sigma_m tan\beta - d \tag{10}$$

Where $d = \sigma_o$, and $tan\beta = \alpha$

Here, β is commonly referred to as the friction angle, which governs the influence of hydrostatic stress on yielding [34, 36]. In practical terms, β controls the slope of the yield surface in the pressure–shear stress space: higher values correspond to stronger pressure dependence, whereas lower values indicate reduced sensitivity. In the specific case of uniaxial tension considered here, the tensile and compressive yield stresses are effectively equal ($\sigma_t = \sigma_c$), which leads to $\alpha=0$ and consequently $\beta=0$. Under this condition, the Drucker–Prager yield criterion simplifies to a von Mises-type, pressure-insensitive formulation, where yielding is governed entirely by the deviatoric stress, and hydrostatic stress has no effect on the onset of plastic deformation. This simplification is fully consistent with the uniaxial tensile tests, where the material response is dominated by shear-driven plastic flow rather than pressure-dependent effects.

The linear Drucker–Prager model further includes the parameter K, defined as the ratio of the yield stress under triaxial tension to that under triaxial compression [33]. This parameter controls the influence of the intermediate principal stress on the shape and orientation of the yield surface. To ensure that the yield surface remains convex—a critical requirement for stable and physically realistic plastic flow—K must satisfy the condition ($0.778 \leq K \leq 1$). Within the context of uniaxial tensile loading, K approaches unity, reflecting the negligible effect of the intermediate principal stress on the material response and supporting the use of a nearly pressure-insensitive, von Mises–type yield behavior.

When plane strain conditions are assumed, the parameter K can be related to the friction angle β using the following expression [41]:

$$K = \frac{1}{1 + \frac{1}{3}\tan\beta} \tag{11}$$

Note that for the present uniaxial tension case, $\tan\beta=0$, which yields K=1. This indicates that the intermediate principal stress has no effect on yielding, and the yield surface reduces to a pressure-insensitive, von Mises-type behavior.

In addition to the yield surface, the linear Drucker–Prager model defines a flow potential function, G, which governs the direction and evolution of plastic strains. In its most general form, G is expressed as follows [34]:

$$G = \sigma_e + \sigma_m\, tan\Psi \tag{12}$$

Here, Ψ denotes the dilation angle, which controls the volumetric component of plastic deformation, and is defined as follows [42]:

$$tan\Psi = \frac{3(1 - 2\upsilon^p)}{2(1 + \upsilon^p)} \tag{13}$$

In this formulation, υ^p represents the plastic Poisson's ratio, which can be obtained experimentally by measuring the evolution of plastic strains in both the longitudinal and transverse directions during tensile loading [34]. For the present study, the dilation angle Ψ angle was set to 100, in agreement with values commonly reported in the literature for polymeric materials [43]. This choice ensures a realistic representation of volumetric plastic strain while maintaining numerical stability in the finite element simulations. It should be emphasized that, in the present study, the friction angle ($\beta=0$) is distinct from the dilation angle ($\Psi = 10^0$), suggesting that a non-associated flow rule was adopted, whereby the direction of plastic flow is defined by the flow potential G rather than the yield surface.

Collectively, the linear Drucker–Prager model parameters for HDPE under uniaxial tensile loading were

defined as follows: the friction angle β was set to 0^0, reflecting the pressure-insensitive, von Mises-type response; the intermediate stress sensitivity parameter K was 1, indicating that the intermediate principal stress has no effect on yielding; and the dilation angle Ψ was assigned a value of 10^0, controlling volumetric plastic deformation within the adopted non-associated flow rule. These parameter selections collectively provide a consistent and robust representation of HDPE's nonlinear tensile behavior in the finite element simulations.

3.2.1 Strain rate dependency

Strain-rate dependency of HDPE was incorporated using the Cowper–Symonds overstress model, expressed as [35]:

$$\sigma_y(\dot{\varepsilon}) = \sigma_0 \left[1 + \left(\frac{\dot{\varepsilon}}{C}\right)^{1/p}\right] \quad (14)$$

where $\sigma_y(\dot{\varepsilon})$is the dynamic yield stress at plastic strain rate $\dot{\varepsilon}$, σ_0 is the quasi-static yield stress measured at the lowest strain rate (5 x 10^{-3} s^{-1} in the preset study), and C and p are the Cowper–Symonds material parameters. Table 2 summarizes the tensile yield strengths of HDPE at different strain rates, which were used to calibrate these parameters. The values of C and p were determined through a least-squares fitting procedure in MATLAB, ensuring accurate representation of the rate-dependent tensile behavior in the finite element simulations. In essence, the least-squares fitting procedure in MATLAB yielded C=0.7 and p=4.48, providing an accurate representation of the strain-rate dependent tensile response in the finite element simulations.

3.2.2 Hardening behavior

The plastic hardening behavior of HDPE was defined based on the experimentally obtained true stress–true strain curve at the lowest strain rate (5 x 10^{-3} s^{-1}). To determine the yield point consistently, the 0.2% offset method was employed, ensuring accurate identification of the initial yield stress and corresponding plastic strain. The resulting curve, which represents the evolution of the true tensile yield stress with increasing plastic strain, is presented in Figure 4(b). This curve was directly used to define the isotropic hardening law in the finite element model, providing a reference for the quasi-static material response. By using the lowest strain-rate data, the hardening behavior serves as the baseline for incorporating strain-rate effects via the Cowper–Symonds model, ensuring that both the initial yield and post-yield plastic flow are accurately captured in the simulations.

In essence, the material properties of HDPE used in the uniaxial tensile test simulations was defined through a combination of elastic, plastic, and rate-dependent parameters, as summarized in Table 1. Elastic properties were assigned based on quasi-static measurements, while the plastic response was described using the hardening curve obtained at the lowest strain rate. Strain-rate effects were incorporated through the Cowper–Symonds model, and the linear Drucker–Prager parameters were calibrated specifically for uniaxial tension. It should be noted that the Drucker–Prager parameters (β and K) used in these simulations are valid only for uniaxial tension and must be recalibrated for multiaxial loading conditions, such as bending or impact, by accounting for the compressive yield stress.

4 Results and discussion

4.1 Experimental results

The true tensile stress–true tensile strain response of HDPE, measured at strain rates ranging from 5 x 10^{-3} to 5 x 10^{-1}, exhibits the characteristic multi-stage behavior of semi-crystalline polymers under uniaxial tension, as shown in Figure 4(a). Initially, the material responds linearly and elastically, dominated by reversible elongation of the amorphous phase. This is followed by a nonlinear regime where plastic deformation begins, associated with fragmentation of crystalline lamellae and cavitation initiated by micro- and nano-void formation within the amorphous regions [15]. With further deformation, cold drawing occurs, characterized by progressive alignment of crystalline lamellae along the loading direction, accompanied by void growth and continued lamellar fragmentation, resulting in stable plastic flow [14, 15]. At higher strains, fibrillar structures approach their maximum extensibility or locking stretch [12], producing pronounced strain hardening and a sharp increase in stress prior to failure. This progression confirms that the experimentally observed tensile behavior of HDPE across the examined strain rate range is consistent with the well-established deformation mechanisms of semi-crystalline polymers [5, 12].

Table 1. Material model properties used in the uniaxial tension test simulations of HDPE.

Parameter	Symbol	Value / Description	Notes
Elastic Modulus	E	801 MPa	From Table 2, quasi-static (5 x 10^{-3} s^{-1})
Poisson's Ratio	ν	0.45 [44]	Isotropic elasticity
Cowper–Symonds Parameter	C	0.7 (Figure 6)	Determined from strain-rate dependent yield data
Cowper–Symonds Exponent	p	4.48 (Figure 6)	Determined from strain-rate dependent yield data
Hardening curve	-	Figure 4(b)	True tensile yield stress–true tensile strain curve at 5 x 10^{-3} s^{-1}, 0.2% offset method
Friction angle	β	0°	Pressure-insensitive, uniaxial tension
Intermediate stress sensitivity	K	1	Plane strain approximation
Dilation angle	Ψ	10° [43]	Non-associated flow rule, controls volumetric plastic strain

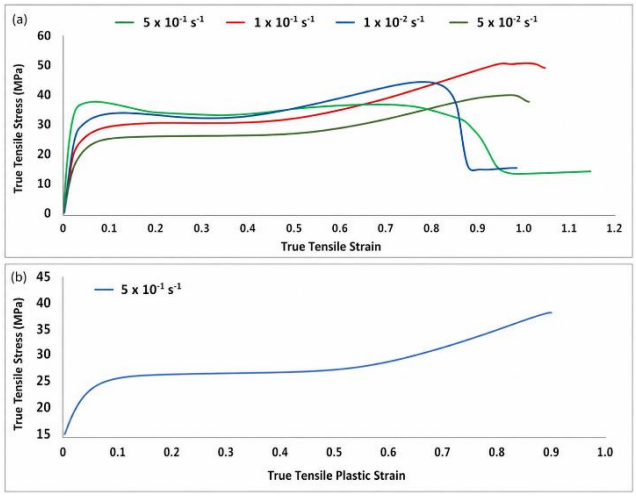

Figure 4. (a) True tensile stress-true tensile strain response of HDPE at various strain rates, and (b) True tensile stress-true tensile plastic strain response of HDPE at 5 x 10^{-3} s^{-1}

The results reported in Table 2 highlights the significant effect of strain rate on the tensile response of HDPE, providing critical insights into its underlying deformation mechanisms. The tensile yield strength nearly doubles, increasing 15.4 ± 0.3 MPa at 5 x 10^{-3} s-1 to 29.7 ± 0.5 MPa at 5 x 10^{-1} s^{-1}, while the tensile elastic modulus rises from 801 ± 20 MPa to 1160 ± 17 MPa, as shown in Figure 5. In contrast, the fracture strain decreases markedly from 1.09 to 0.81, indicating a pronounced loss of ductility at higher strain rates.

Table 2. Variations of tensile yield strength, tensile elastic modulus and fracture strain of HDPE with strain rate.

Strain Rate (s^{-1})	**Tensile Yield Strength (σ_y)** (MPa)	**Tensile Elastic Modulus (E)** (MPa)	Fracture Strain (ε_f)
5 x 10^{-3}	15.4 ± 0.3	801 ± 20	1.09
1 x 10^{-2}	20.6 ± 0.4	938 ± 12	1.06
1 x 10^{-1}	25.4 ± 0.6	1051 ± 18	0.88
5 x 10^{-1}	29.7 ± 0.5	1160 ± 17	0.81

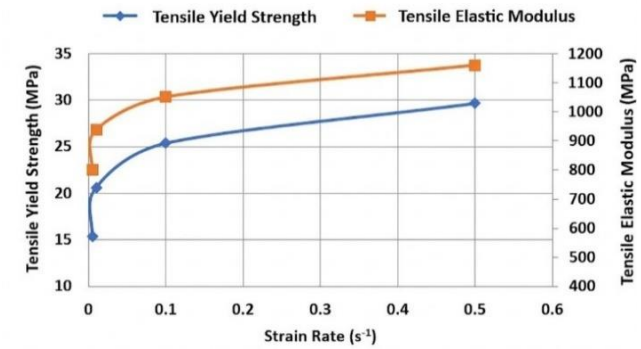

Figure 5. Effect of strain rate on the tensile yield strength and elastic modulus of HDPE.

These observations can be directly linked to the mobility of molecular chains within the semi-crystalline HDPE microstructure. At low strain rates, chains in the amorphous regions can readily uncoil, disentangle, and reorient in response to applied stress, facilitating larger plastic deformation and higher fracture strains [18]. Under faster loading, however, the time available for molecular relaxation is reduced, limiting chain mobility and delaying the ability of amorphous regions to accommodate strain. As a result, stress accumulates more rapidly in both amorphous and crystalline phases, leading to higher yield stresses and elastic stiffness [18]. The reduced chain rearrangement also promotes earlier activation of lamellar slip and cavitation, which, in turn, contributes to the observed reduction in fracture strain at higher rates. Importantly, the quantitative trends in Table 2 reveal a delicate balance between strength and ductility: while the material becomes stronger and stiffer with increasing strain rate, its ability to undergo extensive plastic deformation diminishes.

This interplay reflects the critical role of chain mobility and microstructural reorganization in governing the tensile performance of semi-crystalline polymers. These insights provide a mechanistic basis for understanding HDPE's strain-rate-dependent behavior and underscore the importance of incorporating rate effects in predictive finite element simulations.

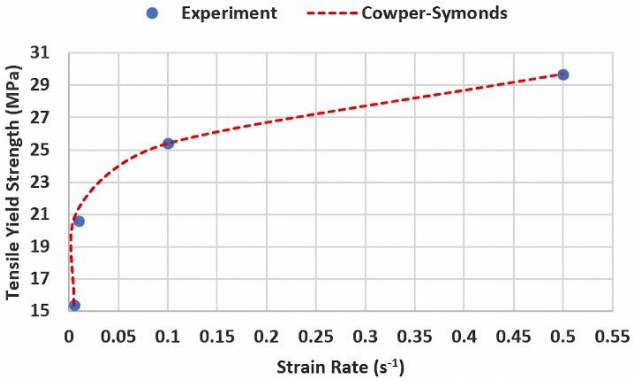

Figure 6. Comparison of the experimentally measured rate-dependent yield strength of HDPE with Cowper-Symonds model predictions.

Figure 6 presents a comparison between the experimentally measured tensile yield strength of HDPE and predictions from the calibrated Cowper–Symonds model across the strain rate range of 5 x 10^{-3} s^{-1} to 5 x 10^{-1} s^{-1}. As shown in Figure 6, the model demonstrates excellent agreement with the experimental data, with deviations remaining below 5% throughout this range. For example, at the lowest strain rate (5 x 10^{-3} s^{-1}), both the experimental and predicted yield strengths are 15.4 MPa, while at the highest strain rate (5 x 10^{-1} s^{-1}), the model predicts 29.69 MPa compared to the experimental value of 29.7 MPa. This close correlation confirms the effectiveness of the Cowper–Symonds overstress formulation in capturing the strain-rate sensitivity of HDPE within the investigated range. It reflects the underlying molecular mechanisms, where increasing

strain rates reduce chain mobility and relaxation, leading to enhanced resistance to plastic deformation. Nevertheless, it should be emphasized that the calibrated Cowper–Symonds parameters are specifically valid for the moderate strain rate range considered in this study. Polymers, including HDPE, can exhibit a pronounced and often nonlinear increase in yield strength at higher strain rates beyond this range, necessitating separate calibration or alternative modeling approaches to accurately predict behavior under extreme loading conditions [45].These findings underscore the model's robustness for finite element simulations of HDPE subjected to strain rates typical of many engineering applications, while also highlighting the need for caution when extrapolating beyond the calibrated domain.

4.2 Finite element analysis results and comparisons

A comparative assessment was performed between the experimentally measured true tensile stress–true tensile strain response of HDPE and the corresponding FEM predictions at three strain rates: $\dot{\varepsilon}$ = 5 x 10^{-3}, $\dot{\varepsilon}$ = 1 x 10^{-1}, and, $\dot{\varepsilon}$ = 5 x 10^{-1} s^{-1}, as shown in Figures 7–9. In addition to the true tensile stress–strain behavior, the normal stress component in the loading direction (S11) was evaluated to characterize the stress distribution and localization within the specimen during deformation.

At the lowest strain rate ($\dot{\varepsilon}$ = 5 x 10^{-3} s^{-1}), the results presented in Figure 7 demonstrate excellent agreement between the experimental measurements and the FEM predictions. The numerical model accurately captures the initial linear elastic region, with a nearly identical slope to that obtained experimentally, confirming the appropriate calibration of the elastic constants in the constitutive model. It is evident from the results presented in Figure 7 that following the onset of yielding, the finite element simulation adequately captures both the yield point and the early stage of strain hardening. However, at larger strain levels, the subsequent hardening response is slightly overestimated compared to the experimental measurements, as illustrated in Figure 7. his deviation remains moderate but becomes more noticeable in the large deformation regime. The observed overprediction of strain hardening can be attributed to limitations of the constitutive model in fully representing the complex deformation mechanisms of HDPE at high strains. In particular, the discrepancy may be attributed to the simplified treatment of strain-induced molecular chain orientation, the absence of progressive damage or microvoid evolution, and the neglect of localized softening mechanisms that occur during advanced stages of neck development. Additionally, potential differences between idealized boundary conditions in the numerical model and the actual experimental constraints may contribute to this slight overestimation.

The S11 stress contours at the lowest strain rate ($\dot{\varepsilon}$ = 5x 10^{-3} s^{-1}), shown in Figure 7, further support the overall mechanical response predicted by the model. During the initial stages of loading, the stress distribution across the gauge section remains nearly uniform, indicating homogeneous deformation and stable load transfer throughout the specimen. As deformation progresses, stress localization gradually intensifies within the central region of the gauge length. This localized stress concentration is consistent with the experimentally observed initiation of necking at the lowest strain rate, demonstrating that the numerical model successfully captures the transition from uniform deformation to localized plastic flow with satisfactory accuracy.

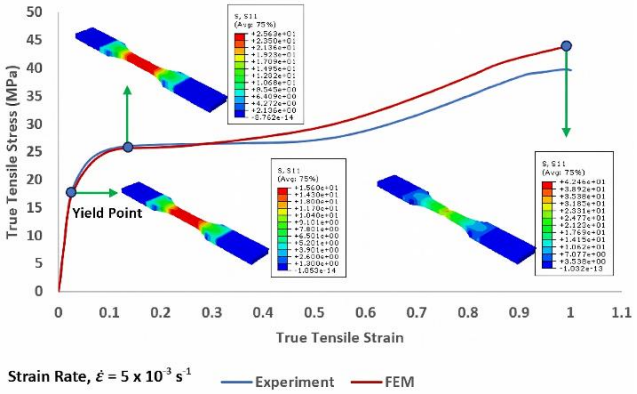

Figure 7. Comparison of the experimentally measured true tensile stress-true tensile strain response of HDPE with FEM predictions at $\dot{\varepsilon}$ = 5 x 10^{-3} s^{-1} and normal stress (S11) contours.

At the intermediate strain rate ($\dot{\varepsilon}$ = 1 x 10^{-1} s^{-1}), the comparison presented in Figure 8 reveals noticeable discrepancies between the experimental response and the finite element predictions. In contrast to the lowest strain rate case, the initial resistance to plastic flow is not reproduced satisfactorily by the implemented linear Drucker–Prager model, as shown in Figure 8. This limitation is primarily attributed to the absence of strain-rate-dependent elastic behavior in the adopted material formulation. As reported in Table 2, the elastic modulus of HDPE increases with strain rate, reflecting its inherent viscoelastic material behavior. However, the present model assumes a rate-independent elastic modulus and does not account for viscoelasticity [6, 22] Consequently, the strain-rate-dependent evolution of stiffness is not captured, representing a significant limitation of the constitutive framework and directly contributing to the discrepancy observed in the elastic–plastic transition region. Furthermore, the finite element model slightly overestimates the yield stress, indicating that the linear Drucker–Prager formulation does not fully capture the material response at this strain rate ($\dot{\varepsilon}$= 1 x 10^{-1} s^{-1}), as shown in Figure 8. Following initial yielding, the post-yield behavior is reproduced qualitatively, but the subsequent strain hardening is overestimated, with deviations increasing at larger strains. This behavior arises because the hardening curve, originally defined at the lowest strain rate (Figure 4(b)), is scaled by the model to account for the imposed strain rate while maintaining its original shape. However, as seen in Figure 4(a), the experimental hardening curve changes shape with strain rate; therefore, simple scaling cannot accurately reproduce the post-yield response. Consequently, both the post-yield stress and the extent of strain hardening are overpredicted, highlighting the limitations of the current

rate-independent hardening formulation and emphasizing the need for a model that captures the strain-rate-dependent evolution of the hardening curve.

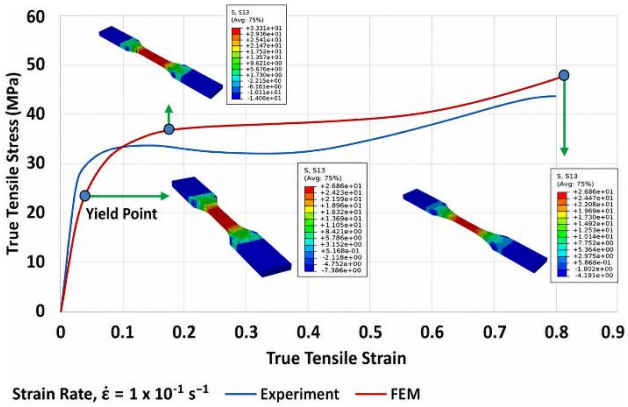

Figure 8. Comparison of the experimentally measured true tensile stress-true tensile strain response of HDPE with FEM predictions at $\dot{\varepsilon}$ = 1 x 10^{-1} s^{-1} and normal stress (S11) contours.

Consequently, both the post-yield stress and the extent of strain hardening are overestimated, reflecting the limitations of the current rate-independent hardening formulation. While approaches such as the Cowper–Symonds model can introduce strain-rate sensitivity for yielding, the present implementation does not account for rate-dependent hardening. As a result, the model overpredicts both the post-yield stress and the magnitude of strain hardening at $\dot{\varepsilon}$ = 1 x 10^{-1} s^{-1}, underscoring the need for a viscoplastic framework capable of capturing not only the initial yielding but also the evolution of the hardening curve under intermediate strain rates.

As shown in Figure 9, at the highest strain rate investigated ($\dot{\varepsilon}$ = 5 x 10^{-1} s^{-1}), the FEM predictions exhibit increased discrepancies compared with the experimentally measured true tensile stress–true tensile strain response, which are more pronounced than at the lower strain rates ($\dot{\varepsilon}$ = 5 x 10^{-3} s^{-1}, and $\dot{\varepsilon}$ = 1 x 10^{-1} s^{-1}). The model overestimates the yield stress, reproduces the post-yield behavior less accurately, and exaggerates the subsequent strain hardening, particularly at larger strains. These limitations arise from the rate-independent nature of the linear Drucker–Prager formulation, which scales the hardening curve defined at the lowest strain rate while maintaining its shape, without accounting for the experimentally observed evolution of hardening with strain rate. While the Cowper–Symonds approach can account for strain-rate sensitivity in yielding, the current implementation lacks rate-dependent hardening. This underscores the need for a viscoplastic framework that can accurately capture both the onset of yielding and the evolution of strain hardening in HDPE under elevated strain rates.

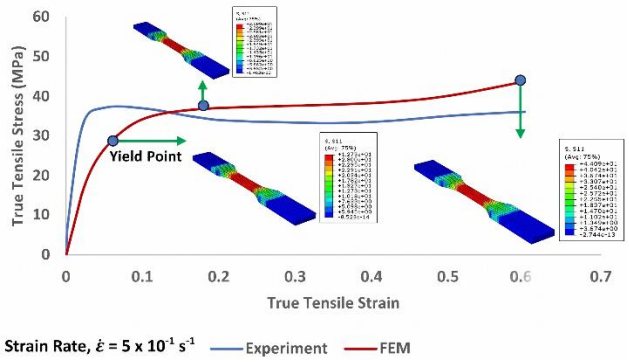

Figure 9. Comparison of the experimentally measured true tensile stress-true tensile strain response of HDPE with FEM predictions at $\dot{\varepsilon}$ = 1 x 10^{-1} s^{-1} and normal stress (S11) contours.

Table 3 presents the percentage error between the experimentally measured true tensile yield stress of HDPE and the corresponding FEM predictions obtained using the linear Drucker–Prager model coupled with the Cowper–Symonds formulation for strain-rate-dependent yielding. The error ratios indicate that the model slightly overestimates the yield stress across all strain rates, with the smallest error of 1.3% at the lowest strain rate ($\dot{\varepsilon}$= 5 x10^{-3} s^{-1}), the largest error of 4.33% at the intermediate strain rate ($\dot{\varepsilon}$ = 1 x 10^{-1} s^{-1}), and a moderate error of 2.69% at the highest experimental strain rate ($\dot{\varepsilon}$ = 5 x 10^{-1} s^{-1}). The results reported in Table 3 clearly reveal that the FEM predictions using the linear Drucker–Prager model coupled with the Cowper–Symonds formulation closely reproduce the strain-rate-dependent yield behavior of HDPE. Minor residual discrepancies are primarily attributed to the rate-independent elastic modulus, which does not capture the experimentally observed stiffening with increasing strain rate. Nevertheless, the Cowper–Symonds approach effectively accounts for the rate sensitivity of yielding, ensuring that the FEM predictions accurately reflect the increase in yield stress across the investigated strain rates. These findings confirm that the key conclusions regarding the rate-dependent yield behavior of HDPE are successfully attained with this combined modeling approach.

Table 3. Comparison of experimentally measured true tensile yield stress of HDPE with FEM predictions at different strain rates.

Strain Rate (s^{-1})	True Tensile Yield Stress (σ_y) (MPa)		Error %
	Experiment	FEM	
5 x 10^{-3}	15.4	15.6 (Figure 7)	1.3
1 x 10^{-1}	25.4	26.5 (Figure 8)	4.33
5 x 10^{-1}	29.7	30.5 (Figure 9)	2.69

Nevertheless, it is worth emphasizing that the yield behavior in the current study was modeled using the Drucker–Prager model with parameters $\beta = 0$ and $K = 1$, which reduces the formulation to the pressure-insensitive Von Mises criterion. This assumption was deliberately adopted to isolate the deviatoric (shear-driven) component of the material response under the considered loading conditions, where shear deformation is dominant. Such a simplification enables a clearer interpretation of the strain rate effects without the additional complexity introduced by hydrostatic pressure dependence. Nevertheless, it is well established that polymers, including High-Density Polyethylene, exhibit pronounced sensitivity to hydrostatic stress.

Therefore, the present formulation represents a limiting case of the more general Drucker–Prager model. Incorporating a non-zero friction angle, calibrated from experimental data available in the literature, would allow for a more realistic representation of pressure-dependent yielding. This highlights the broader capability of the Drucker–Prager model compared to the classical Von Mises formulation and indicates a clear pathway for improving the predictive accuracy of the model in future studies.

Furthermore, the strain rate sensitivity in this study was incorporated using the Cowper–Symonds model, which introduces a rate-dependent scaling of the yield stress while preserving the underlying strain-hardening response. An alternative approach in Abaqus involves the direct implementation of rate-dependent true stress–true plastic strain data in tabular form, allowing an exact reproduction of experimental curves at discrete strain rates. However, such an approach is inherently data-intensive and restricted to the specific strain rate levels for which experimental measurements are available. In contrast, the Cowper–Symonds formulation offers a compact, physically interpretable, and computationally efficient framework that enables a continuous representation of strain rate effects over a broad range using a limited set of material parameters. This capability is particularly critical for parametric investigations and predictive simulations, where extrapolation beyond experimentally tested conditions is often required.

Accordingly, the adoption of the Cowper–Symonds model ensures both robustness and generality in capturing strain rate sensitivity. Nevertheless, the tabular approach is acknowledged as a high-fidelity alternative when extensive experimental datasets are available, and its implementation may further enhance accuracy in future work.

5 Concluding remarks

This study investigated the tensile behavior of HDPE under different strain rates through experiments and finite element simulations. The FEM predictions employed a linear Drucker–Prager material model coupled with the Cowper–Symonds formulation to account for strain-rate-dependent yielding. The experimental results demonstrated that HDPE exhibits strong strain-rate sensitivity, with both the yield strength and elastic modulus increasing from 15.4 MPa and 801 MPa at $\dot{\varepsilon}$ = 5 x 10^{-3} s^{-1} to 29.7 MPa and 1160 MPa at $\dot{\varepsilon}$ = 5 x 10^{-1} s^{-1}, while the fracture strain decreases, indicating reduced ductility at higher loading rates (Table 2). The FEM predictions closely captured the strain-rate-dependent increase in yield stress, with minor overestimations 1.3–4.33% (Table 3), and qualitatively reproduced the post-yield response. However, the model cannot accurately capture the subsequent strain hardening at higher strain rates, as the hardening curve is defined based on the material response at the lowest strain rate ($\dot{\varepsilon}$= 5 x 10^{-3} s^{-1}) and scaled without accounting for changes in its shape with increasing strain rate. Residual discrepancies are also influenced by the rate-independent elastic modulus, which does not reflect the viscoelastic stiffening of HDPE.

Analysis of the S11 stress contours (Figures 7-9) confirmed that the model effectively represents the transition from uniform deformation to localized necking. Overall, these findings demonstrate that the combined linear Drucker–Prager–Cowper–Symonds framework provides a reliable and computationally efficient approach for predicting the rate-dependent yield behavior of HDPE, while highlighting that incorporating rate-dependent hardening and elastic behavior is necessary to fully capture post-yield responses at elevated strain rates.

Conflict of interest

The authors declare that there is no conflict of interest.

Similarity rate (iThenticate): 19%

References

[1] P.J. Alvarado, Steel vs. plastics: The competition for light-vehicle fuel tanks, JOM. 48, 22–25, 1996. https://doi.org/10.1007/BF03222990.

[2] M. Amjadi and A. Fatemi, Tensile behavior of high-density polyethylene including the effects of processing technique, thickness, temperature, and strain rate, Polymers. 12, 1857, 2020. https://doi.org/10.3390/polym12091857.

[3] A. Dasari and R.D.K. Misra, On the strain rate sensitivity of high density polyethylene and polypropylenes, Materials Science and Engineering: A. 358, 356–371, 2003. https://doi.org/10.1016/S0921-5093(03)00330-7.

[4] F. Ohashi, T. Hiroe, K. Fujiwara and H. Matsuo, Strain-rate and temperature effects on the deformation of polypropylene and its simulation under monotonic compression and bending, Polymer Engineering & Science. 42, 1046–1055, 2002. https://doi.org/10.1002/pen.11011.

[5] A. Lamri, M. Shirinbayan, M. Pereira, L. Truffault, J. Fitoussi, S. Lamouri, F. Bakir and A. Tcharkhtchi, Effects of strain rate and temperature on the mechanical behavior of high-density polyethylene, Journal of Applied Polymer Science. 137, 48778, 2020. https://doi.org/10.1002/app.48778.

[6] R. Elleuch and W. Taktak, Viscoelastic behavior of HDPE polymer using tensile and compressive loading, Journal of Materials Engineering and Performance. 15, 111–116, 2006. https://doi.org/10.1361/105994906X83475.

[7] Wiley, Processing and Finishing of Polymeric Materials, 2 Volume Set, John Wiley & Sons, 2012.
[8] D.R. Daniels, T.C.B. McLeish, B.J. Crosby, R.N. Young and C.M. Fernyhough, Molecular Rheology of Comb Polymer Melts. 1. Linear Viscoelastic Response, Macromolecules. 34, 7025–7033, 2001. https://doi.org/10.1021/ma010712p.
[9] J.X. Li and W.L. Cheung, On the deformation mechanisms of β-polypropylene: 1. Effect of necking on β-phase PP crystals, Polymer. 39, 6935–6940, 1998. https://doi.org/10.1016/S0032-3861(98)00144-X.
[10] N. Dusunceli and O.U. Colak, High density polyethylene (HDPE): Experiments and modeling, Mechanics of Time-Dependent Materials. 10, 331–345, 2006. https://doi.org/10.1007/s11043-007-9026-5.
[11] K. Ercan, M.A. Dundar and H.K. Akyildiz, Investigating the flexural behavior of ultra-high-molecular-weight polyethylene at a low bending rate: experimental and numerical study, Mechanics of Solids. 59, 3968–3984, 2024. https://doi.org/10.1134/S0025654424605032.
[12] C.A. Bernard, O. Lame, T. Deplancke, J.-Y. Cavaillé and K. Ogawa, From rheological to original three-dimensional mechanical modelling of semi-crystalline polymers: Application to a wide strain rate range and large deformation of Ultra-High Molecular Weight PolyEthylene, Mechanics of Materials. 151, 103640, 2020. https://doi.org/10.1016/j.mechmat.2020.103640.
[13] B. Xiong, O. Lame, J.-M. Chenal, C. Rochas and R. Seguela, On the strain-induced fibrillar microstructure of polyethylene: Influence of chemical structure, initial morphology and draw temperature, Express Polymer Letters. 10, 311–323, 2016. https://doi.org/10.3144/expresspolymlett.2016.29.
[14] Y. Zhang, P.-Y. Ben Jar, S. Xue and L. Li, Quantification of strain-induced damage in semi-crystalline polymers: a review, Journal of Materials Science. 54, 62–82, 2019. https://doi.org/10.1007/s10853-018-2859-2.
[15] J. Defebvin, S. Barrau, G. Stoclet, C. Rochas and J.-M. Lefebvre, In situ SAXS/WAXS investigation of the structural evolution of poly(vinylidene fluoride) upon uniaxial stretching, Polymer. 84, 148–157, 2016. https://doi.org/10.1016/j.polymer.2015.12.041.
[16] J.M.L. Reis, L.J. Pacheco and H.S. da Costa Mattos, Influence of the temperature and strain rate on the tensile behavior of post-consumer recycled high-density polyethylene, Polymer Testing. 32, 1576–1581, 2013. https://doi.org/10.1016/j.polymertesting.2013.10.008.
[17] A. Lamri, M. Shirinbayan, M. Pereira, L. Truffault, J. Fitoussi, S. Lamouri, F. Bakir and A. Tcharkhtchi, Effects of strain rate and temperature on the mechanical behavior of high-density polyethylene, Journal of Applied Polymer Science. 137, 48778, 2020. https://doi.org/10.1002/app.48778.
[18] M. Amjadi and A. Fatemi, Tensile behavior of high-density polyethylene including the effects of processing technique, thickness, temperature, and strain rate, Polymers. 12, 1857, 2020. https://doi.org/10.3390/polym12091857.
[19] A. Dasari and R.D.K. Misra, On the strain rate sensitivity of high density polyethylene and polypropylenes, Materials Science and Engineering: A. 358, 356–371, 2003. https://doi.org/10.1016/S0921-5093(03)00330-7.
[20] J.M.L. Reis, L.J. Pacheco and H.S. da Costa Mattos, Tensile behavior of post-consumer recycled high-density polyethylene at different strain rates, Polymer Testing. 32, 338–342, 2013. https://doi.org/10.1016/j.polymertesting.2012.11.007.
[21] N. Dusunceli and O.U. Colak, High density polyethylene (HDPE): Experiments and modeling, Mechanics of Time-Dependent Materials. 10, 331–345, 2006. https://doi.org/10.1007/s11043-007-9026-5.
[22] N. Dusunceli and O.U. Colak, The effects of manufacturing techniques on viscoelastic and viscoplastic behavior of high density polyethylene (HDPE), Materials & Design. 29, 1117–1124, 2008. https://doi.org/10.1016/j.matdes.2007.06.003.
[23] ASTM D638-14, Standard Test Method for Tensile Properties of Plastics, 2015.
[24] D. Grommes, O. Bruch and J. Geilen, Investigation of the influencing factors on the process-dependent elasticity modulus in extrusion blow molded plastic containers for material modelling in the finite element simulation, in: AIP Conf. Proc., AIP Publishing LLC, 2016, p. 050013. https://doi.org/10.1063/1.4965518.
[25] S.M. Kurtz, L. Pruitt, C.W. Jewett, R. Paul Crawford, D.J. Crane and A.A. Edidin, The yielding, plastic flow, and fracture behavior of ultra-high molecular weight polyethylene used in total joint replacements, Biomaterials. 19, 1989–2003, 1998. https://doi.org/10.1016/S0142-9612(98)00112-4.
[26] S.M. Kurtz, M.L. Villarraga, M.P. Herr, J.S. Bergström, C.M. Rimnac and A.A. Edidin, Thermomechanical behavior of virgin and highly crosslinked ultra-high molecular weight polyethylene used in total joint replacements, Biomaterials. 23, 3681–3697, 2002. https://doi.org/10.1016/S0142-9612(02)00102-3.
[27] L.G. Malito, The Deformation, Yielding, and Fracture of Ultra-High Molecular Weight Polyethylene for Use in Total Joint Replacements, University of California, Berkeley, 2018.
[28] S.M. Kurtz, M.L. Villarraga, M.P. Herr, J.S. Bergström, C.M. Rimnac and A.A. Edidin, Thermomechanical behavior of virgin and highly crosslinked ultra-high molecular weight polyethylene used in total joint replacements, Biomaterials. 23, 3681–3697, 2002. https://doi.org/10.1016/S0142-9612(02)00102-3.
[29] S.M. Kurtz, L. Pruitt, C.W. Jewett, R. Paul Crawford, D.J. Crane and A.A. Edidin, The yielding, plastic flow, and fracture behavior of ultra-high molecular weight polyethylene used in total joint replacements, Biomaterials. 19, 1989–2003, 1998. https://doi.org/10.1016/S0142-9612(98)00112-4.
[30] C. G'Sell, S. Boni and S. Shrivastava, Application of the plane simple shear test for determination of the

plastic behaviour of solid polymers at large strains, Journal of Materials Science. 18, 903–918, 1983. https://doi.org/10.1007/BF00745590.
[31] C. G'Sell, J.M. Hiver, A. Dahoun and A. Souahi, Video-controlled tensile testing of polymers and metals beyond the necking point, Journal of Materials Science. 27, 5031–5039, 1992. https://doi.org/10.1007/BF01105270.
[32] C. G'Sell and J.J. Jonas, Determination of the plastic behaviour of solid polymers at constant true strain rate, Journal of Materials Science. 14, 583–591, 1979. https://doi.org/10.1007/BF00772717.
[33] D. Systèmes, ABAQUS Documentation (Dassault Systèmes, Providence, RI), 2014.
[34] M.A. Dundar and O. Ozenc, Examining the effect of dilation angle on the flexural response of amorphous polymers using finite element analysis, Multidiscipline Modeling in Materials and Structures. 1–14, 2025. https://doi.org/10.1108/MMMS-03-2025-0097.
[35] M.A. Dundar, Assessing the effectiveness of the linear Drucker–Prager material model in predicting the mechanical behavior of acrylonitrile–butadiene–styrene (ABS) under multiaxial loading conditions, Polymer Engineering & Science. 65, 1283–1310, 2025. https://doi.org/10.1002/pen.27075.
[36] G. Dean and L. Wright, An evaluation of the use of finite element analysis for predicting the deformation of plastics under impact loading, Polymer Testing. 22, 625–631, 2003. https://doi.org/10.1016/S0142-9418(02)00168-X.
[37] D. Forni, B. Chiaia and E. Cadoni, Strain rate behaviour in tension of S355 steel: Base for progressive collapse analysis, Engineering Structures. 119, 164–173, 2016. https://doi.org/10.1016/j.engstruct.2016.04.013.
[38] D. Systèmes, Abaqus Analysis User's Manual: Element Library, Dassault Systèmes, 2016.
[39] G. Dean and L. Crocker, The Use of Finite Element Methods for Design with Adhesives, Measurement Good Practice Guide, 2001.
[40] Y. Duan, A. Saigal, R. Greif and M.A. Zimmerman, Impact behavior and modeling of engineering polymers, Polymer Engineering & Science. 43, 112–124, 2003. https://doi.org/10.1002/pen.10010.
[41] O. Ozenc, M.A. Dundar and D.E. Sahin, Examination of compressive and flexural behaviors of acrylonitrile-butadiene-styrene filled with hemp fiber particles, Journal of Thermoplastic Composite Materials. 37, 743–771, 2023. https://doi.org/10.1177/08927057231186326.
[42] G. Quino, J. Gargiuli, S. Pimenta, I. Hamerton, P. Robinson and R.S. Trask, Experimental characterisation of the dilation angle of polymers, Polymer Testing. 125, 108137, 2023. https://doi.org/10.1016/j.polymertesting.2023.108137.
[43] G. Quino, J. Gargiuli, S. Pimenta, I. Hamerton, P. Robinson and R.S. Trask, Experimental characterisation of the dilation angle of polymers, Polymer Testing. 125, 1–7, 2023. https://doi.org/10.1016/j.polymertesting.2023.108137.
[44] J. Pelto, V. Heino, M. Karttunen, I. Rytöluoto and H. Ronkainen, Tribological performance of high density polyethylene (HDPE) composites with low nanofiller loading, Wear. 460–461, 203451, 2020. https://doi.org/10.1016/j.wear.2020.203451.
[45] S.M. Walley and J.E. Field, Strain rate sensitivity of polymers in compression from low to high rates, DYMAT Journal. 1, 211–227, 1994.